Hindawi Publishing Corporation
International Journal of Spectroscopy
Volume 2010, Article ID 371201, 11 pages
doi:10.1155/2010/371201

Research Article

Collision-Induced Infrared Absorption by Molecular Hydrogen Pairs at Thousands of Kelvin

Xiaoping Li,[1] Katharine L. C. Hunt,[1] Fei Wang,[2] Martin Abel,[2] and Lothar Frommhold[2]

[1] *Department of Chemistry, Michigan State University, East Lansing, MI 48824, USA*
[2] *Physics Department, University of Texas, Austin, TX 78712-1081, USA*

Correspondence should be addressed to Lothar Frommhold, frommhold@physics.utexas.edu

Received 21 April 2009; Accepted 18 July 2009

Academic Editor: Chantal Stehle

Collision-induced absorption by hydrogen and helium in the stellar atmospheres of cool white dwarfs causes the emission spectra to differ significantly from the expected blackbody spectra of the cores. For detailed modeling of radiative processes at temperatures up to 7000 K, the existing H_2–H_2 induced dipole and potential energy surfaces of high quality must be supplemented by calculations with the H_2 bonds stretched or compressed far from the equilibrium length. In this work, we describe new dipole and energy surfaces, based on more than 20 000 *ab initio* calculations for H_2–H_2. Our results agree well with previous *ab initio* work (where those data exist); the calculated rototranslational absorption spectrum at 297.5 K matches experiment similarly well. We further report the calculated absorption spectra of H_2–H_2 for frequencies from the far infrared to 20 000 cm^{-1}, at temperatures of 600 K, 1000 K, and 2000 K, for which there are no experimental data.

1. Introduction

It is well known that dense gases of infrared inactive molecules such as H_2 absorb infrared radiation. Absorption continua range from the microwave and far infrared regions of the spectrum to the near infrared and possibly into the visible. Collisionally interacting pairs of hydrogen molecules possess transient electric dipole moments, which are responsible for the observed absorption continua [1, 2]. Planetary scientists understood early on the significance of collision-induced absorption (CIA) for the modeling of the atmospheres of the outer planets [3, 4]. More recently, it was shown that the emission spectrum of cool white dwarf stars differs significantly from the expected blackbody spectrum of their cores: CIA in the dense helium and hydrogen atmospheres suppresses (filters) the infrared emissions strongly [5–10]. Detailed modelling of the atmospheres of cool stars with proper accounting for the collision-induced opacities is desirable, but it has been hampered heretofore by the highly incomplete or nonexisting theoretical and experimental data on such opacities at temperatures of many thousands of kelvin.

Quantum chemical calculations of the induced dipole surfaces of H_2–H_2, H_2–He and other complexes have been very successful [11–14]. Based on such data, molecular scattering calculations accounting for the interactions of the molecular complexes with photons have been undertaken which accurately reproduced the existing laboratory measurements at low temperatures ($T \leq 300$ K or so) [2]. At higher temperatures, virtually no suitable laboratory measurements of such opacities exist, but reliable data are needed. We therefore decided to extend such quantum chemical calculations of the induced dipole (ID) and potential energy surfaces (PES) of H_2–H_2 complexes to highly rotovibrationally excited molecules, as encountered at high temperatures (up to 7 000 K) and photon energies up to ~2.5 eV.

2. *Ab Initio* Calculations of the Induced Dipole and Potential Energy Surfaces

At the temperatures characteristic of cool white-dwarf atmospheres, the CIA spectra depend on transition dipole

matrix elements with vibrational quantum numbers up to $v \approx 7$. To evaluate these matrix elements, we have determined the induced dipoles and interaction energies of pairs of hydrogen molecules with bond lengths ranging from 0.942 a.u. to 2.801 a.u. (1 a.u. = $a_0 = 5.29177249 \cdot 10^{-11}$ m). For comparison, the vibrationally averaged internuclear separation in H_2 is 1.449 a.u., in the ground vibrational state. We have used MOLPRO 2000 [15] to calculate the PES for H_2–H_2 and to calculate the pair ID by finite-field methods, at coupled-cluster single and double excitation level, with triple excitations treated perturbatively [CCSD(T)]. In this work, we have employed MOLPRO's aug-cc-pV5Z(spdf) basis, consisting of (9s 5p 4d 3f) primitive Gaussians contracted to [6s 5p 4d 3f]; this gives 124 contracted basis functions for each of the H_2 molecules. The basis gives accurate energies and properties [16]; yet it is sufficiently compact to permit calculations on H_2 pairs with 28 different combinations of H_2 bond lengths, at 7 different intermolecular separations, in 17 different relative orientations (the orientations listed in Table 1), and at a minimum of 6 different applied field strengths for each geometrical configuration.

In the calculations, the centers of mass of the two H_2 molecules are separated along the Z axis by distances R ranging from 4.0 to 10.0 a.u. The vector **R** joins molecule 2 to molecule 1. The molecular orientations are characterized by the angles $(\theta_1, \theta_2, \varphi_{12})$, where θ_1 is the angle between the Z axis and the symmetry axis of molecule 1, θ_2 is the angle between the Z axis and the symmetry axis of molecule 2, and φ_{12} is the dihedral angle between two planes, one defined by the Z axis and the symmetry axis of molecule 1 and the other defined by the Z axis and the symmetry axis of molecule 2.

Calculations were performed first for two molecules with bond lengths of $r_1 = r_2 = 1.449$ a.u., the ground-state, vibrationally averaged internuclear separation. The interaction energies were evaluated in the absence of an applied field; then the pair dipoles were obtained from finite-field calculations, grouped into three sets of 40. Within each of the sets, the fields were confined to the XY, XZ, or YZ planes, and the two components of the applied field were selected randomly, in the range from 0.001 a.u. to 0.01 a.u., for a total of 120 calculations. For each fixed set of the bond lengths, orientation angles, and intermolecular separation, the total energies were fit (by least squares) to a quartic polynomial in the applied field **F**:

$$E = E_0 - \mu_\alpha F_\alpha - \left(\frac{1}{2}\right)\alpha_{\alpha\beta}F_\alpha F_\beta - \frac{1}{6}\beta_{\alpha\beta\gamma}F_\alpha F_\beta F_\gamma - \frac{1}{24}\gamma_{\alpha\beta\gamma\delta}F_\alpha F_\beta F_\gamma F_\delta - \cdots, \quad (1)$$

where the Einstein convention of summation over repeated Greek subscripts is followed. The coefficients of the linear terms were selected from each fit, to obtain the Cartesian components of the induced dipole moments μ_X, μ_Y, and μ_Z. In Table 1, our results for the components of the pair dipole are given for pairs with $r_1 = r_2 = 1.449$ a.u.

In earlier work on the polarizabilities α for H_2–H_2 [16], we conducted several tests of this fitting procedure: we compared results from quartic fits with 120 different field strengths, quartic fits with 200 different field strengths, and quintic and sixth-order fits with 200 field strengths (at one set of orientation angles and an intermolecular distance of 2.5 a.u., where the differences between the calculations were expected to be magnified); we found excellent agreement among the results from all of the fits. We also compared the results from the random-field calculations with the values obtained analytically, based on calculations with 6 or 8 selected values of the field strengths, for fixed orientation angles and the full range of intermolecular separations. The field values were grouped into the sets $\{f, 2^{1/2}f, 3^{1/2}f, -f, -2^{1/2}f, -3^{1/2}f\}$, $\{f, 2^{1/2}f, 5^{1/2}f, -f, -2^{1/2}f, -5^{1/2}f\}$, and $\{f, 2^{1/2}f, 3^{1/2}f, 5^{1/2}f, -f, -2^{1/2}f, -3^{1/2}f, -5^{1/2}f\}$, with $f = 0.001$, 0.002, 0.003, and 0.004 a.u. At the shortest intermolecular distance ($R = 2.5$ a.u.), the results for $f = 0.001$ a.u. – 0.003 a.u. were affected by numerical imprecision in the hyperpolarization contributions; at larger R, they agreed well with the random-field results. Agreement between the random-field results and the results obtained with $f = 0.004$ a.u. was excellent for all R values. On this basis, we have used random-field fits in the work with $r_1 = r_2 = 1.449$ a.u., but we have used analytic fits with 6 different field values for the computations with r_1 or $r_2 \neq 1.449$ a.u. In [16], we also compared the results obtained via analytic differentiation at the self-consistent field (SCF) level using Gaussian 98 versus the results from our SCF calculations, for the full range of intermolecular separations and three different relative orientations, again with excellent agreement. Basis set superposition error (BSSE) has been shown to be negligible [16], as tested by function counterpoise ("ghost-orbital") methods. BSSE occurs when the pair basis provides a better representation of H_2–H_2 than the single-molecule basis provides for an isolated H_2 molecule. In these calculations, BSSE has been suppressed by the large size of the single-molecule basis.

The interaction mechanisms that determine the induced dipole include classical multipole polarization, van der Waals dispersion, and short-range exchange, overlap, and orbital distortion. At long range, the leading term in the collision-induced dipole comes from quadrupolar induction, which varies as R^{-4} in the separation R between the molecular centers [2]. The next long-range polarization term is of order R^{-6}; it results both from hexadecapolar induction and from the effects of the nonuniformity of the local field gradient (due to the quadrupole moment of the collision partner). The magnitude of the latter term depends on the dipole-octopole polarizability tensor E. At order R^{-7}, back-induction [17, 18] and dispersion [17–21] affect the pair dipole. Back-induction is a static reaction field effect: the field from the permanent quadrupole of molecule 1 polarizes molecule 2, which sets up a reaction field that polarizes molecule 1 (and similarly, with molecules 1 and 2 interchanged). The van der Waals dispersion dipole results from *dynamic* reaction-field effects, combined with the effects of an applied, static field [21], via two physical mechanisms.

Table 1: Cartesian components μ_X, μ_Y, and μ_Z of the H_2–H_2 dipole in a.u. (multiplied by 10^6) with bond lengths $r_1 = r_2 = 1.449$ a.u.

R (a.u.)	4.0	5.0	6.0	7.0	8.0	9.0	10.0
$(\theta_1, \theta_2, \varphi_{12})$				μx			
$(\pi/12, \pi/6, \pi/3)$	48	150	103	63	39	25	16
$(\pi/12, \pi/4, \pi/6)$	−3675	−2393	−1393	−804	−480	−299	−195
$(\pi/12, \pi/3, \pi/6)$	−2790	−1791	−1044	−607	−366	−230	−150
$(\pi/12, 5\pi/12, \pi/6)$	−144	−28	−17	−16	−15	−11	−8
$(\pi/6, \pi/4, \pi/3)$	1417	1294	806	471	280	175	115
$(\pi/6, \pi/3, \pi/4)$	399	562	365	210	121	74	49
$(\pi/6, 5\pi/12, \pi/3)$	2065	1922	1196	695	411	255	167
$(\pi/4, \pi/3, \pi/6)$	1109	879	528	302	177	109	72
$(\pi/4, 5\pi/12, \pi/6)$	3481	2432	1424	815	481	299	195
$(\pi/3, 5\pi/12, \pi/6)$	2555	1804	1062	611	363	226	148
$(7\pi/12, \pi/12, \pi/6)$	−7979	−5226	−3027	−1740	−1037	−648	−424
$(7\pi/12, \pi/6, \pi/4)$	−9089	−5973	−3462	−1988	−1184	−740	−484
$(7\pi/12, \pi/4, \pi/6)$	−11040	−7181	−4151	−2381	−1417	−885	−580
$(7\pi/12, \pi/3, \pi/6)$	−9759	−6345	−3669	−2107	−1255	−785	−515
$(\pi/2, \pi/12, \pi/6)$	−3628	−2337	−1341	−765	−452	−282	−184
$(\pi/2, \pi/6, \pi/3)$	−3575	−2303	−1322	−754	−447	−278	−182
$(\pi/2, \pi/4, \pi/6)$	−7071	−4535	−2606	−1489	−884	−551	−361
				μ_Y			
$(\pi/12, \pi/6, \pi/3)$	−6236	−4288	−2519	−1453	−864	−539	−352
$(\pi/12, \pi/4, \pi/6)$	−3691	−2635	−1566	−908	−542	−338	−221
$(\pi/12, \pi/3, \pi/6)$	−2801	−2088	−1257	−733	−440	−275	−180
$(\pi/12, 5\pi/12, \pi/6)$	−1060	−952	−599	−355	−214	−135	−88
$(\pi/6, \pi/4, \pi/3)$	−5443	−4082	−2455	−1429	−854	−533	−349
$(\pi/6, \pi/3, \pi/4)$	−2847	−2414	−1496	−880	−529	−332	−217
$(\pi/6, 5\pi/12, \pi/3)$	−1427	−1430	−916	−545	−330	−207	−136
$(\pi/4, \pi/3, \pi/6)$	−1008	−1209	−793	−473	−286	−179	−117
$(\pi/4, 5\pi/12, \pi/6)$	419	−239	−224	−145	−90	−57	−37
$(\pi/3, 5\pi/12, \pi/6)$	404	−211	−199	−127	−78	−49	−32
$(7\pi/12, \pi/12, \pi/6)$	−997	−877	−543	−317	−189	−118	−77
$(7\pi/12, \pi/6, \pi/4)$	−2588	−2187	−1342	−780	−464	−290	−189
$(7\pi/12, \pi/4, \pi/6)$	−2416	−1890	−1142	−662	−394	−246	−161
$(7\pi/12, \pi/3, \pi/6)$	−2415	−1757	−1045	−604	−360	−225	−147
$(\pi/2, \pi/12, \pi/6)$	−835	−798	−501	−294	−175	−109	−71
$(\pi/2, \pi/6, \pi/3)$	−2521	−2367	−1481	−865	−515	−321	−210
$(\pi/2, \pi/4, \pi/6)$	−1734	−1570	−976	−569	−339	−211	−138
				μ_Z			
$(\pi/12, \pi/6, \pi/3)$	−15702	−5371	−2141	−1026	−568	−345	−223
$(\pi/12, \pi/4, \pi/6)$	−35330	−12145	−4900	−2374	−1322	−808	−525
$(\pi/12, \pi/3, \pi/6)$	−53105	−18342	−7486	−3664	−2053	−1258	−820
$(\pi/12, 5\pi/12, \pi/6)$	−65061	−22550	−9278	−4573	−2574	−1580	−1032
$(\pi/6, \pi/4, \pi/3)$	−19683	−6793	−2764	−1349	−755	−463	−301
$(\pi/6, \pi/3, \pi/4)$	−37478	−13007	−5355	−2641	−1486	−914	−597
$(\pi/6, 5\pi/12, \pi/3)$	−49514	−17248	−7156	−3553	−2008	−1237	−810
$(\pi/4, \pi/3, \pi/6)$	−17837	−6231	−2596	−1293	−731	−451	−296
$(\pi/4, 5\pi/12, \pi/6)$	−29903	−10485	−4400	−2205	−1253	−774	−509
$(\pi/3, 5\pi/12, \pi/6)$	−12057	−4257	−1805	−913	−522	−323	−213
$(7\pi/12, \pi/12, \pi/6)$	65301	22600	9286	4573	2573	1580	1032
$(7\pi/12, \pi/6, \pi/4)$	49757	17294	7161	3553	2008	1237	810
$(7\pi/12, \pi/4, \pi/6)$	30125	10528	4404	2206	1253	775	510

Table 1: Continued.

R (a.u.)	4.0	5.0	6.0	7.0	8.0	9.0	10.0
$(7\pi/12, \pi/3, \pi/6)$	12133	4272	1807	914	522	323	214
$(\pi/2, \pi/12, \pi/6)$	69310	24042	9916	4898	2761	1697	1109
$(\pi/2, \pi/6, \pi/3)$	53764	18746	7796	3879	2196	1354	887
$(\pi/2, \pi/4, \pi/6)$	34212	11998	5042	2532	1441	891	58

(1) Spontaneous, quantum mechanical fluctuations in the charge density of molecule 1 produce a fluctuating field that acts on molecule 2; then molecule 2 is hyperpolarized by the concerted action of the field from 1 and the applied field **F**. This sets up a field-dependent dynamic reaction field at molecule 1, giving a term in the van der Waals energy that is linear in the applied field **F**. (2) The correlations of the fluctuations in the charge density of molecule 1 are altered by the static field **F** acting on 1; molecule 2 responds linearly to field-induced changes in the fluctuations of the charge density of 1, again giving a term in the van der Waals energy that is linear in the applied field **F**. The precise functional forms of the short-range exchange, overlap, and orbital-distortion effects on the dipole are not known; however, these contributions are expected to drop off (roughly) exponentially with increasing R [2].

The dipole moment of the pair can be cast into a symmetry-adapted form, as a series in the spherical harmonics of the orientation angles of molecules 1 and 2 and the orientation angles of the intermolecular vector:

$$\begin{aligned}\mu_1{}^M(\mathbf{R}, \mathbf{r}_1, \mathbf{r}_2) = (4\pi)^{3/2}\ 3^{-1/2} \sum A_{\lambda_1\lambda_2\Lambda L}(R, r_1, r_2) \\ \times Y_{\lambda_1}{}^{m_1}(\Omega_1) Y_{\lambda_2}{}^{m_2}(\Omega_2) Y_L{}^{M-m}(\Omega_R) \\ \times \langle \lambda_1\lambda_2 m_1 m_2 \mid \Lambda m\rangle \langle \Lambda L m(M-m) \mid 1M\rangle,\end{aligned} \tag{2}$$

where the sum runs over all values of $\lambda_1, \lambda_2, m_1, m_2, \Lambda$ and m; $M = 1, 0$, or -1, corresponding to the dipole components,

$$\begin{aligned}\mu_1{}^1 &= -\left(\frac{1}{2}\right)^{1/2}\left(\mu_X + i\mu_Y\right), \\ \mu_1{}^0 &= \mu_Z, \\ \mu_1{}^{-1} &= \left(\frac{1}{2}\right)^{1/2}(\mu_X - i\mu_Y).\end{aligned} \tag{3}$$

In (2), Ω_1 and Ω_2 denote the orientation angles of molecules 1 and 2, that is, the orientation angles of the z axes of the molecule-fixed frames, Ω_R is the orientation angle of the vector **R** (note that **R** runs from molecule 2 to molecule 1, in this work), and the quantities $\langle \lambda_1\lambda_2 m_1 m_2 \mid \Lambda m\rangle$ and $\langle \Lambda L M(M-m) \mid 1M\rangle$ are Clebsch-Gordan coefficients. Equation (2) follows immediately from the fact that the collision-induced dipole of H_2–H_2 is a first-rank spherical tensor, which is obtained by coupling functions of $\mathbf{r}_1$, $\mathbf{r}_2$, and **R**. Therefore λ_1, λ_2, Λ, L, and the magnitudes of $\mathbf{r}_1$, $\mathbf{r}_2$, and **R** completely determine the dipole expansion coefficients $A_{\lambda_1\lambda_2\Lambda L}(R, r_1, r_2)$.

The dipole coefficients arising from various long-range polarization mechanisms are categorized in Table 2, through order R^{-7}. In this table, Θ denotes the molecular quadrupole moment; $\overline{\alpha}$ is the trace of the single-molecule polarizability; $\alpha_\parallel - \alpha_\perp$ is the polarizability anisotropy, which is equal to $\alpha_{zz} - \alpha_{xx}$ in the molecular axis system, where z is the symmetry axis; Φ is the hexadecapole moment; E is the dipole-octopole polarizability, which has a second-rank spherical tensor component E_2 and a fourth-rank component E_4. The van der Waals dispersion dipole is given by an integral over imaginary frequencies, where the integrand is a product of the polarizability at imaginary frequency $\alpha(i\omega)$ and the dipole-dipole-quadrupole hyperpolarizability $B(0, i\omega)$. The B tensor is a fourth-rank Cartesian tensor with spherical-tensor components of ranks 0, 2, and 4.

For distinct molecules 1 and 2, or for chemically identical molecules that have different bond lengths, all of the dipole coefficients listed in Table 2 are nonzero, although some of the coefficients may be quite small numerically. For chemically identical molecules, when $r_1 = r_2$, the coefficients A_{0001}, $A_{22\Lambda 1}$ with $\Lambda \neq 1$, $A_{22\Lambda 3}$ with $\Lambda \neq 3$, and A_{2245} vanish; the remainder are nonzero. The coefficients $A_{0\lambda\lambda L}$ and $A_{24\Lambda L}$ can be obtained from the coefficients $A_{\lambda 0\lambda L}$ and $A_{42\Lambda L}$ via the relations

$$\begin{aligned}A_{0\lambda\lambda L} &= -\mathcal{P}^{12}\mathrm{A}_{\lambda 0\lambda \mathrm{L}}, \\ A_{24\Lambda L} &= (-1)^{\Lambda+1}\mathcal{P}^{12}A_{42\Lambda L},\end{aligned} \tag{4}$$

where $\mathcal{P}^{12}$ interchanges the labels of molecules 1 and 2. For centrosymmetric molecules such as H_2, the dipole coefficients $A_{\lambda\lambda'\Lambda L}$ vanish unless λ and λ' are both even. Also, due to the Clebsch-Gordan coefficients in (2), nonvanishing contributions are found only if $\Lambda = L-1$, L, or $L+1$. Coefficients with higher values of λ and λ' than those listed are of higher order than R^{-7} at long-range, although they may represent significant short-range overlap effects.

From the dipole values in Table 1, we have obtained a set of A coefficients by least-squares fit (at each R value) to (2), for $r_1 = r_2 = 1.449$ a.u. From the fit, we have been able to determine the coefficients A_{2021}, A_{0221}, A_{2023}, A_{0223}, A_{2211}, A_{2233}, A_{4043}, A_{0443}, A_{4045}, A_{0445}, A_{4221}, A_{2421}, A_{4223}, A_{2423}, A_{4233}, A_{2433}, A_{4243}, A_{2443}, A_{4245}, A_{2445}, A_{4255}, A_{2455}, A_{4265}, A_{2465}, A_{4267}, and A_{2467}. We have kept all of these coefficients, as well as A_{0001} and A_{2201}, in the calculations with unequal bond lengths for molecules 1 and 2. However, for $R \geq 4.0$ a.u and $r_1 = r_2 = 1.449$ a.u., the least squares fit shows that the first ten coefficients are numerically important, while the remaining coefficients are essentially negligible. At $R = 4.0$ a.u., the remaining coefficients do not exceed $7.0 \cdot 10^{-5}$ a.u. in absolute value, and the values drop off

Table 2: Long-range dipole induction mechanisms that contribute to the coefficients $A_{\lambda\lambda'\Lambda L}$ of (2) for a pair of molecules A and B [17, 18].

Induction mechanism	Power law	Properties	Coefficients
Quadrupolar field	R^{-4}	Θ, $\overline{\alpha}$	A_{2023}, A_{0223}
		Θ, $\alpha_\parallel - \alpha_\perp$	$A_{22\Lambda 3}$, $\Lambda = 2, 3, 4$
Hexadecapolar field	R^{-6}	Φ, $\overline{\alpha}$	A_{4045}, A_{0445}
		Φ, $\alpha_\parallel - \alpha_\perp$	$A_{42\Lambda 5}$, $\Lambda = 4, 5, 6$
			$A_{24\Lambda 5}$, $\Lambda = 4, 5, 6$
Nonuniform field gradient	R^{-6}	Θ, E_2	A_{2245}
		Θ, E_4	$A_{42\Lambda 5}$, $\Lambda = 4, 5, 6$
			$A_{24\Lambda 5}$, $\Lambda = 4, 5, 6$
Back-induction	R^{-7}	Θ, $\overline{\alpha}$, $\alpha_\parallel - \alpha_\perp$	A_{0001}
			A_{2021}, A_{0221}
			A_{2023}, A_{0223}
			A_{2221}
			$A_{22\Lambda 3}$, $\Lambda = 2, 3, 4$
			A_{2245}
			A_{4043}, A_{0443}
		Θ, $\alpha_\parallel - \alpha_\perp$	A_{2021}, A_{0221}
			A_{2023}, A_{0223}
			$A_{22\Lambda 1}$, $\Lambda = 0, 1, 2$
			$A_{22\Lambda 3}$, $\Lambda = 2, 3, 4$
			A_{2245}
			A_{4221}, A_{2421}
			$A_{42\Lambda 3}$, $\Lambda = 2, 3, 4$
			$A_{24\Lambda 3}$, $\Lambda = 2, 3, 4$
			$A_{42\Lambda 5}$, $\Lambda = 4, 5, 6$
			$A_{24\Lambda 5}$, $\Lambda = 4, 5, 6$
Dispersion	R^{-7}	$\overline{\alpha}\,(i\omega)$, $B_0(0, i\omega)$	A_{0001}
		$\overline{\alpha}\,(i\omega)$, $B_2(0, i\omega)$	A_{2021}, A_{0221}
			A_{2023}, A_{0223}
		$\alpha_\parallel(i\omega) - \alpha_\perp(i\omega)$, $B_0(0, i\omega)$	A_{2021}, A_{0221}
			A_{2023}, A_{0223}
		$\overline{\alpha}(i\omega)$, $B_4(0, i\omega)$	A_{4043}, A_{0443}
		$\alpha_\parallel(i\omega) - \alpha_\perp(i\omega)$, $B_2(0, i\omega)$	$A_{22\Lambda 1}$, $\Lambda = 0, 1, 2$
			$A_{22\Lambda 3}$, $\Lambda = 2, 3, 4$
			A_{2245}
		$\alpha_\parallel(i\omega) - \alpha_\perp(i\omega)$, $B_4(0, i\omega)$	A_{4221}, A_{2421}
			$A_{42\Lambda 3}$, $\Lambda = 2, 3, 4$
			$A_{24\Lambda 3}$, $\Lambda = 2, 3, 4$
			$A_{42\Lambda 5}$, $\Lambda = 4, 5, 6$
			$A_{24\Lambda 5}$, $\Lambda = 4, 5, 6$

rapidly with increasing R. Table 3 gives our results for A_{2021}, A_{2023}, A_{2211}, A_{2233}, A_{4043}, and A_{4045}; the other numerically significant coefficients are given by the relations $A_{0221} = -A_{2021}$, $A_{0223} = -A_{2023}$, $A_{0443} = -A_{4043}$, and $A_{0445} = -A_{4045}$.

In Table 3, the results are also compared with results from two earlier *ab initio* calculations of the H_2–H_2 dipole with $r_1 = r_2 = 1.449$ a.u., reported by Meyer et al. [12], Meyer et al. [13], and Fu et al. [22]. (The signs in Table 3 follow from our choice of the positive direction of the intermolecular vector **R**.) Meyer et al. [12, 13] used configuration-interaction wave functions including single, double, and triple excitations from a reference Slater determinant, in a (7s 1p) basis of Gaussian primitives on each H center, contracted to [3s 1p] and augmented by a (3s, 2p, 2d) basis at the center of the H–H bond, giving a total of 31 basis functions for H_2 [11]. They performed calculations for 18 relative orientations that provided 9 nonredundant Cartesian dipole components. Fu et al. [22] employed the same basis to generate the CCSD (T) wave functions, in calculations for H_2–H_2 in 13 relative orientations, selected so that $\mu_Y = 0$ in all cases. To find the dipoles, they used finite-field methods, with two fields that were equal in magnitude but opposite in sign. From Table 3,

Table 3: Dipole expansion coefficients $A_{\lambda\lambda' \Lambda L}$ (in a.u., multiplied by 10^6) for H_2–H_2 with $r_1 = r_2 = 1.449$ a.u. Results from this calculation, compared with results of Meyer et al. [13] (MBF), Fu et al. [22] (FZB), long-range results [17, 18] through order R^{-7}(LR), and quadrupole-induced dipole coefficients (QID).

	R (a.u.)	4.0	5.0	6.0	7.0	8.0	9.0	10.0
A_{2021}	This work	9983	2123	407	73	13	4	2
	MBF	10401	2190	429	84	20	7	—
	FZB	10385	2184	427	83	19	6	—
	LR	279	59	16	6	2	1	0
A_{2023}	This work	−20065	−8076	−3725	−1950	−1124	−695	−455
	MBF	−19967	−7953	−3688	−1939	−1119	−692	—
	FZB	−19949	−7946	−3685	−1938	−1118	−692	—
	LR	−19687	−7652	−3603	−1921	−1118	−695	−455
	QID	−17628	−7221	−3482	−1880	−1102	−688	−451
A_{2211}	This work	402	86	18	3	0	0	0
	MBF	332	74	14	2	0	0	—
	FZB	332	74	14	2	0	0	—
	LR	−41	−9	−2	−1	0	0	0
A_{2233}	This work	2020	977	514	289	171	107	70
	MBF	1992	949	498	280	166	104	—
	FZB	1991	949	498	279	166	104	—
	LR	2588	1088	530	288	169	106	70
	QID	2726	1117	538	291	170	106	70
A_{4043}	This work	690	180	42	9	2	0	0
	LR	204	43	12	4	2	1	0
A_{4045}	This work	−845	−283	−97	−37	−16	−8	−4
	MBF	−1523	−450	−135	−47	−19	−9	—
	FZB	−1517	−447	−134	−46	−19	−9	—
	LR	−1040	−273	−91	−36	−16	−8	−4

it is apparent that the results of Fu et al. (FZB) [22] agree well with the earlier results given by Meyer et al. (MBF) [13].

For the largest coefficients, A_{2023} and A_{0223}, our results are in excellent agreement with both of the earlier calculations: The percent differences between our results and those of Meyer et al. [13] are largest at $R = 5.0$ a.u. (1.52%) and $R = 6.0$ a.u. (0.99%); the remaining differences in these two coefficients average to 0.48%. We have obtained results at $R = 10.0$ a.u., which were not given previously. The differences between our values for A_{2233} and those of Meyer et al. [13] are typically ∼3% (smaller at $R = 4.0$ a.u.). Differences in the values of A_{2021} and A_{0221} are ∼5% or less at short range ($R \leq 6.0$ a.u.), where these coefficients have their largest values. At longer range, the absolute discrepancies are smaller, although the differences are larger on a relative basis. The principal differences in the dipole coefficients are attributable to the inclusion of A_{4043} and A_{0443} in our work; this affects the values of A_{4045}, A_{0445}, and A_{2211} (to a lesser extent).

In Table 3, the *ab initio* values of the coefficients are also compared with values based on the quadrupole-induced dipole model (QID) and the long range model (LR), which is complete through order R^{-7}. The LR calculations include hexadecapolar induction, back-induction, and van der Waals dispersion effects, in addition to quadrupolar induction. The QID and LR calculations are based on the value of the H_2 quadrupole computed by Poll and Wolniewicz [23], the value of Θ interpolated to $r = 1.449$ a.u. given by Visser et al. [24], the hexadecapole computed by Karl et al. [25], the polarizabilities and E-tensor values given by Bishop and Pipin [26], and the dispersion dipoles computed from the polarizability and dipole-dipole-quadrupole polarizability at imaginary frequencies, also given by Bishop and Pipin [27].

The coefficient A_{2023} depends primarily on the quadrupole-induced dipole: the difference between the QID approximation and our result is ∼12% at $R = 4.0$ a.u., ∼10.6% at $R = 5.0$ a.u., ∼6.5% for $R = 6.0$ a.u., and smaller at larger R. The QID model gives remarkably good values for this coefficient, even when R is quite small. Agreement with the full long-range model is somewhat better, with errors of ∼5.25% at $R = 5.0$ a.u. and only 1.88% at $R = 4.0$ a.u. Quadrupole-induced dipole effects are also present in the coefficient A_{2233}; this coefficient fits the QID and LR models quite well for $R \geq 6.0$ a.u., but the percent errors in these approximations are larger than those in A_{2023} for $R = 4.0$ and 5.0 a.u. It should be noted that the back-induction and dispersion contributions have the same sign in A_{2023} but opposite signs in A_{2233}.

At long range the values of A_{4045} and A_{0445} depend on hexadecapolar induction, which varies as R^{-6}; there are no other contributions through order R^{-7}. We find strong agreement between the values of these coefficients and the hexadecapole-induced dipole terms (which determine LR),

for $R \geq 5.0$ a.u.; short-range effects become significant when R is reduced to 4.0 a.u. In contrast, A_{2021}, A_{0221}, A_{2211}, A_{4043}, and A_{0443} seem to reflect the short-range exchange, overlap, and orbital distortion effects predominantly. For these coefficients, the leading long-range terms of back-induction and dispersion vary as R^{-7}; and they contribute with opposite signs in each case, further reducing the net effect of the long-range polarization mechanisms, in these particular dipole coefficients.

As noted above, we have carried out calculations with 28 different combinations of bond lengths in molecules 1 and 2. *Ab initio* calculations have been completed for pairs with each bond length combination, in each of the 17 relative orientations, at each of 7 separations between the centers of mass, and for at least six values of the applied field in the X, Y, or Z direction.

In the work of Meyer et al. on the absorption spectra of H_2–H_2 pairs in the fundamental band, results for the Cartesian components of the pair dipoles are listed for four nonredundant pairs of bond lengths, (r_o, r_o), (r_o, r_-), (r_o, r_+), and (r_-, r_+), with r_o = 1.449 a.u., r_- = 1.111 a.u., and r_+ = 1.787 a.u. [13]. Fu et al. [22] augmented this set by the addition of a larger bond length, r_{++} = 2.150 a.u., and reported results for all ten nonredundant pairs of configurations with the bond lengths drawn from the set $\{r_o, r_-, r_+, r_{++}\}$. In the current work, we have included r_o, three bond lengths smaller than r_o (1.280 a.u., 1.111 a.u., and 0.942 a.u.), and four bond lengths larger than r_o (1.787 a.u., 2.125 a.u., 2.463 a.u., and 2.801 a.u.), in order to examine new portions of the dipole surface, particularly those that may become significant for photon absorption at higher temperatures. The specific nonredundant length combinations used in the calculations are (r_1, r_2) = (2.801, 2.125), (2.801, 1.787), (2.801, 1.449), (2.801, 1.280), (2.801, 1.111), (2.801, 0.942), (2.463, 2.125), (2.463, 1.787), (2.463, 1.449), (2.463, 1.280), (2.463, 1.111), (2.463, 0.942), (2.125, 1.787), (2.125, 1.449), (2.125, 1.280), (2.125, 1.111), (2.125, 0.942), (1.787, 1.449), (1.787, 1.280), (1.787, 1.111), (1.787, 0.942), (1.449, 1.449), (1.449, 1.280), (1.449, 1.111), (1.449, 0.942), (1.280, 1.111), (1.280, 0.942), and (1.111, 0.942), with all bond lengths in a.u.

To illustrate the results for pairs with one or both bond lengths displaced from r_o (the averaged internuclear separation in the ground vibrational state of H_2), in Table 4 we list our values for the dipole expansion coefficients when r_1 = 1.787 a.u. and r_2 = 1.449 a.u., and we compare with the values given earlier by Fu et al. [22]. In general, we find excellent agreement. The values of A_{0001}, A_{2021}, A_{0221}, A_{2023}, A_{0223}, A_{2233}, A_{2243}, and A_{2245} agree quite closely, particularly given the extension of the basis set and the corrections for hyperpolarization effects included in the current work. A few of the coefficients show larger differences, based on differences in the fitting procedures. In the current work, we have omitted the coefficients A_{2221} and A_{2223}, which were included by Fu et al.; this contributes to the difference in the fitted values of A_{2211}. On the other hand, we have included A_{4043} and A_{0443}, which were omitted by Fu et al. [22]; this probably accounts for the difference in the values of A_{4045} and A_{0445} shown in Table 4. Our inclusion of A_{4221}, A_{2421}, A_{4223}, A_{2423}, A_{4243}, A_{2443}, A_{4245}, A_{2445}, A_{4265}, A_{2465}, A_{4267}, and A_{2467} in the fitting procedure also causes slight shifts in the values of the other coefficients.

No previous results are available for comparison when one or both of the molecules in the pair have bond lengths of 0.942 a.u., 1.280 a.u., 2.125 a.u, 2.463 a.u., or 2.801 a.u. In Table 5, we provide results for one such combination of bond lengths, with r_1 = 2.463 a.u. and r_2 = 1.787 a.u. The coefficients listed in the top line of each set (and the corresponding coefficients for other pairs of bond lengths) were used in generating the rototranslational and vibrational spectra. These were obtained from fits that included 26 dipole coefficients all together (with A_{2211} and A_{2233}, but not A_{2221} and A_{2223}); immediately below those results in each set, we list values obtained from fits with 27 dipole coefficients (including A_{2221} and A_{2223}, but not A_{2211}). We find that the coefficients A_{0001}, A_{2021}, A_{2023}, A_{2243}, A_{2245}, A_{4043}, and A_{4045} are numerically "robust;" these coefficients are little affected by the difference in the fitting procedure. The coefficients A_{0221}, A_{0223}, A_{2233}, A_{0443}, and A_{0445} show greater sensitivity, although the agreement tends to improve as the separation between the molecular centers R increases (particularly for A_{0223} and A_{2233}). The full results for the new potential energy surface and the pair dipoles, with individual H_2 bond lengths ranging from 0.942 a.u. to 2.801 a.u., will be reported and analyzed in a subsequent paper. However, here we note that the coefficients A_{2023}, A_{0223}, A_{2233}, A_{4045}, and A_{0445} appear to be dominated by long-range induction mechanisms, specifically quadrupolar induction for A_{2023}, A_{0223}, and A_{2233}, hexadecapolar induction for A_{4045} and A_{0445}, and E-tensor induction for A_{2245}. When the logarithms of the absolute values of these coefficients are plotted versus the logarithms of the separations R between the molecular centers of mass, over the range from 8.0 a.u. to 10.0 a.u., the slopes are −4.20 for A_{2023}, −4.08 for A_{0223}, and −3.995 for A_{2233}, all close to the quadrupolar-induction value of −4. Similarly, the slopes are −6.42 for A_{4045} and −6.34 for A_{0445}, close to the value of −6 for hexadecapolar induction; and the slope is −5.84 for A_{2245}, close to the value of −6 for E-tensor induction [17].

3. About the Spectra

The absorption spectrum is a quasicontinuum, consisting of many thousand highly diffuse, unresolved "lines," corresponding to rotovibrational transitions from an initial state $\{\nu_1, j_1, \nu_2, j_2\}$, to a final state $\{\nu_1', j_1', \nu_2', j_2'\}$, of the binary collision complex. Under the conditions encountered in cool stellar atmospheres, vibrational quantum numbers ν from 0 to about 5 occur with significant population numbers, with rotational quantum numbers j up to 20 or so, for H_2 molecules.

The isotropic potential approximation (IPA), which neglects the anisotropic terms of the intermolecular potential, is used for the calculation of the spectra [2]. Each "line" requires as input the matrix elements of the spherical dipole components [2]

$$\langle \nu_1 j_1 \nu_2 j_2 \mid A_{\lambda_1\lambda_2\Lambda L}(R, r_1, r_2) \mid \nu_1' j_1' \nu_2' j_2' \rangle, \qquad (5)$$

Table 4: Dipole expansion coefficients $A_{\lambda\lambda'\Lambda L}$ (in a.u., multiplied by 10^6) for H_2–H_2 with $r_1 = 1.787$ a.u. and r_2=1.449 a.u. The results from this calculation are compared with the results of Fu et al. (FZB), [22].

	R (a.u.)	4.0	5.0	6.0	7.0	8.0	9.0	10.0
A_{0001}	This work	−22960	−5786	−1241	−203	−10	13	9
	FZB	−21869	−5518	−1232	−231	−29	6	—
A_{2021}	This work	20653	4618	928	168	26	2	1
	FZB	21290	4688	963	194	45	15	—
A_{0221}	This work	−10595	−2394	−486	−95	−16	−1	−2
	FZB	−11028	−2450	−508	−108	−28	−10	—
A_{2023}	This work	−32456	−12335	−5392	−2735	−1554	−957	−624
	FZB	−32287	−12113	−5368	−2749	−1568	−966	—
A_{0223}	This work	23916	10071	4764	2525	1459	905	591
	FZB	23778	9865	4685	2488	1439	889	—
A_{2211}	This work	733	166	37	7	0	−2	0
	FZB	528	126	26	3	0	0	—
A_{2233}	This work	3079	1497	789	443	260	161	106
	FZB	2952	1415	750	423	253	158	—
A_{2243}	This work	−316	−242	−150	−88	−55	−34	−23
	FZB	−375	−263	−148	−83	−49	−30	—
A_{2245}	This work	416	180	86	39	19	10	5
	FZB	433	184	72	29	13	6	—
A_{4043}	This work	1981	529	123	29	8	3	1
A_{0443}	This work	−623	−185	−43	−9	0	1	0
A_{4045}	This work	−2079	−684	−224	−84	−35	−16	−9
	FZB	−3956	−1129	−322	−108	−43	−20	—
A_{0445}	This work	989	364	131	53	23	12	5
	FZB	1559	524	169	61	25	11	—

and the isotropic component of the intermolecular potential for the initial (unprimed) state

$$\langle \nu_1 j_1 \nu_2 j_2 \mid V_{000}(R, r_1, r_2) \mid \nu_1 j_1 \nu_2 j_2 \rangle; \quad (6)$$

the potential for the final state is given by a similar expression, where all rotovibrational quantum numbers are primed. The line shape calculations proceed with these expressions as described elsewhere [2]. In (5), (6), as above, R designates the intermolecular separation and r_1, r_2 the intramolecular separations. The indices $\lambda_1\lambda_2\Lambda L$ are the expansion parameters of the spherical dipole components in (2).

Figure 1 shows the calculated absorption coefficient $\alpha(\nu; T)$, normalized by the numerical density ρ squared, at the temperature T of 297.5 K, and frequencies ν from 0 to 3000 cm^{-1} (the "rototranslational band"). Laboratory measurements [28] are shown for comparison (•). Good agreement of theory and measurements is observed.

We note that similarly good agreement of theory and measurement was previously observed, based on an earlier *ab initio* ID surface and a refined intermolecular potential [2, 12]. In the present work, a more complete induced dipole surface has been obtained and used, although the extension has not significantly affected the rototranslational band, shown in Figure 1. Additionally, a new potential energy surface has been obtained and used in the current work. This new potential surface (as well as the new ID surface) accounts for highly rotovibrationally excited H_2 molecules; and the new surfaces will be essential for our high-temperature opacity calculations—but again, the extensions of the potential surface are of little consequence for the rototranslational band, Figure 1, near room temperature.

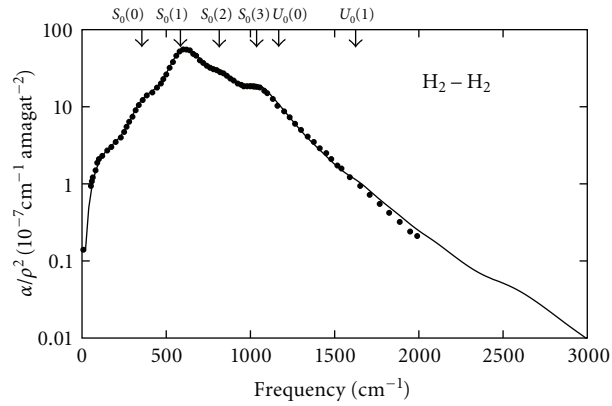

Figure 1: The calculated absorption spectrum of pairs of molecular hydrogen in the rototranslational band of H_2, at the temperature of 297.5 K, and comparison with laboratory measurements (• from [28]).

The new potential surface is believed to be accurate in the repulsive region of the interaction, but it is not as

Table 5: Dipole expansion coefficients $A_{\lambda\lambda'\Lambda L}$ (in a.u., multiplied by 10^6) for H_2-H_2 with $r_1 = 2.463$ a.u. and $r_2 = 1.787$ a.u. Results from the fit used to calculate the spectra (top line in each set) are compared with an alternate fit, which includes A_{2221} and A_{2223}, but not A_{2211}.

R (a.u.)	4.0	5.0	6.0	7.0	8.0	9.0	10.0
A_{0001}	−67727	−18429	−4357	−863	−119	8	14
	−65778	−19365	−4616	−960	−112	22	25
A_{2021}	61278	16009	3620	734	126	12	−3
	61859	15730	3543	705	128	16	0.5
A_{0221}	−23618	−6192	−1472	−322	−60	−9	−1
	−14285	−4351	−1033	−235	−47	−10	−1
A_{2023}	−77947	−28920	−11520	−5413	−2954	−1786	−1157
	−78659	−28577	−11425	−5378	−2956	−1791	−1161
A_{0223}	47485	20508	9741	5119	2948	1819	1185
	53866	22606	10265	5251	2955	1809	1178
A_{2211}	2759	674	164	37	4	−2	−1
A_{2221}	9063	937	201	10	16	8	7
A_{2223}	3803	2494	642	187	1	−19	−15
A_{2233}	6468	3571	1978	1144	678	424	278
	−2544	1369	1441	1024	666	430	282
A_{2243}	−1604	−788	−575	−362	−223	−143	−94
	−1711	−737	−561	−357	−223	−143	−95
A_{2245}	4102	1139	545	266	129	66	35
	4222	1082	530	260	129	67	36
A_{4043}	8512	2914	742	175	45	14	5
	8404	2966	756	181	44	13	4
A_{0443}	−1310	−616	−178	−41	−8	0	1
	−1531	−510	−149	−30	−8	−2	−1
A_{4045}	−7655	−3106	−984	−339	−134	−62	−32
	−7534	−3165	−1000	−345	−133	−61	−31
A_{0445}	2393	1086	415	162	70	33	17
	2640	968	382	150	71	35	19

extensively modeled in the well region, and at long range (dispersion part). Nevertheless, the measurements of the absorption spectra are as closely reproduced by the new *ab initio* input, Figure 1, as they are by the earlier advanced models. Apparently, the collision-induced absorption spectra arise mainly through interactions in the repulsive part of the potential, which is certainly consistent with previous observations [2].

The new opacity calculations of the fundamental and H_2 overtone bands [29] show similar agreement with measurements. Figure 2 shows the calculated normalized absorption coefficients over a frequency band ranging from the microwave region of the spectrum to the visible. In these calculations, we have used the exact equilibrium populations for the initial states, which at 2000 K consist of $v = 0$, 1, and 2, with many different rotational states, including highly excited states. For the final states (after a photon of energy up to 2.5 eV has been absorbed), we have included much higher rotovibrational states of the molecules. We have accounted for all of these states rigorously, using the new intermolecular potential and induced dipole surfaces.

The coarse structures seen in the spectrum correspond roughly to the rototranslational band (peak near 600 cm^{-1}), the fundamental band of H_2 (peak near 4200 cm^{-1}), and the first through fourth overtone bands of H_2 (remaining peaks). Unfortunately, no measurements exist for these high-frequency data, but we feel that the results shown are of comparable reliability to the results in Figure 1.

Calculations of the type shown supplement previous estimates, especially at the highest frequencies [10, 30]. Presently, we are attempting calculations of H_2–H_2 opacities at still higher temperatures (up to 7000 K). Moreover, similar calculations are planned for H_2-He and H_2-H collisional complexes.

4. Conclusion

We report opacity calculations of collisional H_2–H_2 complexes for temperatures of thousands of kelvin and a frequency range from the microwave to the visible regions of the electromagnetic spectrum. The calculations are based on new *ab initio* induced dipole and potential energy surfaces of rotovibrating H_2 molecules, and are intended to facilitate modeling the atmospheres of cool stars. Agreement with earlier theoretical work and laboratory measurements, where these exist, is excellent.

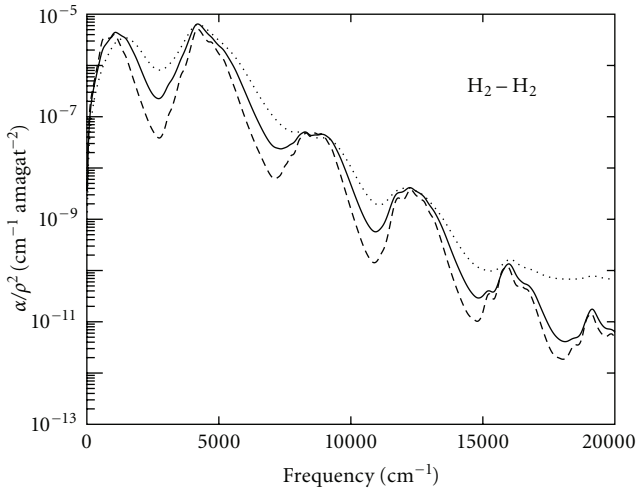

Figure 2: Calculated absorption spectrum of pairs of molecular hydrogen, from the far infrared to the visible, at the temperatures of 600 K (dashes), 1000 K (solid line), and 2000 K (dotted).

Acknowledgments

This work has been supported in part by the National Science Foundation Grants AST-0709106 and AST-0708496 and by the National Natural Science Foundation of China Grant NSFC-10804008.

References

[1] H. L. Welsh, "Pressure induced absorption spectra of hydrogen," in *MTP International Review of Science. Physical Chemistry, Series One, Vol. III: Spectroscopy*, A. D. Buckingham and D. A. Ramsay, Eds., chapter 3, pp. 33–71, Butterworths, London, UK, 1972.

[2] L. Frommhold, *Collision-Induced Absorption in Gases*, Cambridge University Press, Cambridge, UK, 2006.

[3] L. M. Trafton, "The thermal opacity in the major planets," *Astrophysical Journal*, vol. 140, p. 1340, 1964.

[4] L. M. Trafton, "Planetary atmospheres: the role of collision-induced absorption," in *Molecular Complexes in Earth's, Planetary, Cometary, and Interstellar Atmospheres*, A. A. Vigasin and Z. Slanina, Eds., pp. 177–193, World Scientific, Singapore, 1998.

[5] J. Mould and J. Liebert, "Infrared photometry and atmospheric composition of cool white-dwarfs," *Astrophysical Journal*, vol. 226, pp. L29–L33, 1978.

[6] P. Bergeron, D. Saumon, and F. Wesemael, "New model atmospheres for very cool white dwarfs with mixed H/He and pure He compositions," *Astrophysical Journal*, vol. 443, no. 2, pp. 764–779, 1995.

[7] B. M. S. Hansen, "Old and blue white-dwarf stars as a detectable source of microlensing events," *Nature*, vol. 394, no. 6696, pp. 860–862, 1998.

[8] D. Saumon and S. B. Jacobson, "Pure hydrogen model atmospheres for very cool white dwarfs," *Astrophysical Journal*, vol. 511, no. 2, pp. L107–L110, 1999.

[9] P. Bergeron, S. K. Leggett, and M. T. Ruiz, "Photometric and spectroscopic analysis of cool white dwarfs with trigonometric parallax measurements," *The Astrophysical Journal, Supplement Series*, vol. 133, no. 2, pp. 413–449, 2001.

[10] A. Borysow, U. G. Jørgensen, and Y. Fu, "High-temperature (1000–7000 K) collision-induced absorption of H_2 pairs computed from the first principles, with application to cool and dense stellar atmospheres," *Journal of Quantitative Spectroscopy and Radiative Transfer*, vol. 68, no. 3, pp. 235–255, 2001.

[11] W. Meyer and L. Frommhold, "Collision-induced rototranslational spectra of H_2-He from an accurate *ab initio* dipole moment surface," *Physical Review A*, vol. 34, no. 4, pp. 2771–2779, 1986.

[12] W. Meyer, L. Frommhold, and G. Birnbaum, "Rototranslational absorption spectra of H_2-H_2 pairs in the far infrared," *Physical Review A*, vol. 39, no. 5, pp. 2434–2448, 1989.

[13] W. Meyer, A. Borysow, and L. Frommhold, "Absorption spectra of H_2-H_2 pairs in the fundamental band," *Physical Review A*, vol. 40, no. 12, pp. 6931–6949, 1989.

[14] W. Meyer, A. Borysow, and L. Frommhold, "Collision-induced first overtone band of gaseous hydrogen from first principles," *Physical Review A*, vol. 47, no. 5, pp. 4065–4077, 1993.

[15] H.-J. Werner, P. J. Knowles, J. Almlöf, et al., *MOLPRO, Version 2000.1*, Universität Stuttgart, Stuttgart, Germany and Cardiff University, Cardiff, UK, 2000.

[16] X. Li, C. Ahuja, J. F. Harrison, and K. L. C. Hunt, "The collision-induced polarizability of a pair of hydrogen molecules," *Journal of Chemical Physics*, vol. 126, no. 21, Article ID 214302, 2007.

[17] J. E. Bohr and K. L. C. Hunt, "Dipoles induced by long-range interactions between centrosymmetric linear molecules: theory and numerical results for $H_2 \ldots H_2$, $H_2 \ldots N_2$, and $N_2 \ldots N_2$," *The Journal of Chemical Physics*, vol. 87, no. 7, pp. 3821–3832, 1987.

[18] X. Li and K. L. C. Hunt, "Transient, collision-induced dipoles in pairs of centrosymmetric, linear molecules at long range: Results from spherical-tensor analysis," *The Journal of Chemical Physics*, vol. 100, no. 12, pp. 9276–9278, 1994.

[19] K. L. C. Hunt, "Long-range dipoles, quadrupoles, and hyperpolarizabilities of interacting inert-gas atoms," *Chemical Physics Letters*, vol. 70, no. 2, pp. 336–342, 1980.

[20] L. Galatry and T. Gharbi, "The long-range dipole moment of two interacting spherical systems," *Chemical Physics Letters*, vol. 75, pp. 427–433, 1980.

[21] K. L. C. Hunt and J. E. Bohr, "Effects of van der Waals interactions on molecular dipole moments: The role of field-induced fluctuation correlations," *The Journal of Chemical Physics*, vol. 83, no. 10, pp. 5198–5202, 1985.

[22] Y. Fu, Ch. Zheng, and A. Borysow, "Quantum mechanical computations of collision-induced absorption in the second overtone band of hydrogen," *Journal of Quantitative Spectroscopy and Radiative Transfer*, vol. 67, no. 4, pp. 303–321, 2000.

[23] J. D. Poll and L. Wolniewicz, "The quadrupole moment of the H_2 molecule," *The Journal of Chemical Physics*, vol. 68, no. 7, pp. 3053–3058, 1978.

[24] F. Visser, P. E. S. Wormer, and W. P. J. H. Jacobs, "The nonempirical calculation of second-order molecular properties by means of effective states. III. Correlated dynamic polarizabilities and dispersion coefficients for He, Ne, H_2, N_2, and O_2," *The Journal of Chemical Physics*, vol. 82, no. 8, pp. 3753–3764, 1985.

[25] G. Karl, J. D. Poll, and L. Wolniewicz, "Multipole moments of hydrogen molecule," *Canadian Journal of Physics*, vol. 53, pp. 1781–1790, 1975.

[26] D. M. Bishop and J. Pipin, "Dipole, quadrupole, octupole, and dipole octupole polarizabilities at real and imaginary frequencies for H, He, and H_2 and the dispersion-energy coefficients for interactions between them," *International Journal of Quantum Chemistry*, vol. 45, pp. 349–361, 1993.

[27] D. M. Bishop and J. S. Pipin, "Calculation of the dispersion-dipole coefficients for interactions between H, He, and H_2," *The Journal of Chemical Physics*, vol. 98, no. 5, pp. 4003–4008, 1993.

[28] G. Bachet, E. R. Cohen, P. Dore, and G. Birnbaum, "The translational rotational absorption spectrum of hydrogen," *Canadian Journal of Physics*, vol. 61, no. 4, pp. 591–603, 1983.

[29] M. Abel and L. Frommhold, To be published.

[30] A. Borysow, U. G. Jørgensen, and Ch. Zheng, "Model atmospheres of cool, low-metallicity stars: The importance of collision-induced absorption," *Astronomy and Astrophysics*, vol. 324, no. 1, pp. 185–195, 1997.